An Adaptive Multilevel Approach to the Minimal Compliance Problem in Topology Optimization *

Roman Stainko

Special Research Program SFB F013

'Numerical and Symbolic Scientific Computing'

Johannes Kepler University Linz

roman.stainko@sfb013.uni-linz.ac.at

Abstract

This paper presents a new solution strategy for a standard topology optimization problem: the minimal compliance problem. This problem contains the system of linear elasticity partial differential equations (PDEs) as a constraint resulting in a large scaled optimization problem after the finite element discretization. Due to the repeated solution of the direct field problem given by the PDE constraints, efficient solution techniques are required. In this paper we present a new solution method involving adaptive multilevel techniques. Topology optimization problems are ill-posed, so regularization is needed. In our algorithm we combine two regularization techniques, in fact filter methods, such that their disadvantages are eliminated and only their positive properties remain. Numerical experiments are performed with several benchmark problems, where our multilevel approach turns out to be quite efficient. For solving the optimization problems arising in each iteration step, the method of moving asymptotes is used.

Keywords: Topology Optimization, Minimal Compliance, Filter Methods, Adaptive Mesh-Refinement, Multilevel Approach.

1 Introduction

For the development and design process of new products or structures it is of great importance to find the best possible layout. However it is basically unclear how to choose the initial topology, i.e., where to place material and where to place holes. Also due to the fact

---

that the topology is crucial for finding the optimal layout, it pays off to start the design process with optimizing the basic layout. So it turned out that in the recent decade the field of topology optimization, although it is relatively new, is rapidly expanding with an enormous development in terms of theory, computational methods and applications including commercial applications (e.g., Optistruct by Altair, http://www.altair.com). A comprehensive review of the field of structural optimization is given in the monographs by ALLAIRE [2], BENDSØE [3], BENDSØE AND SIGMUND [4], and HASLINGER AND NEITTAANMÄKI [11], and in the survey articles by ESCHENAUER AND OLHOFF [10] and ROZVANY [14]. All contain many references on the various aspects of this field of optimization in general.

This paper deals with a multilevel approach to minimal compliance problems. In these problems an optimal material distribution is searched with respect to maximal stiffness and restriction of the total volume used. Minimizing compliance turned out to be a standard problem in topology optimization. However it already contains the most basic, but non-trivial difficulties like mesh dependent solutions, local minima and checkerboard phenomena.

The remainder of this paper is organized as follows. In the next section an introduction to topology optimization by means of minimizing compliance is given. In the following section some aspects of topology optimizations are treated, namely material interpolation and regularization. Then our adaptive multilevel algorithm is introduced and motivated by the considerations of the previous section. The efficiency of this hierarchical approach is illustrated by our numerical examples, presented in the next section. Finally, conclusions are drawn and some plans for the future improvements are discussed.

2   The Minimal Compliance Problem

This section gives an introduction to the field of topology optimization on the basis of the so-called minimal compliance problem (MCP). The MCP aims at the design of the stiffest (or least compliant) structure under a given fixed load, possible support conditions and restriction on the volume of the used material.

The beginning of this section is devoted to the equation that determines the state of equilibrium of a structure under applied external forces. In the following, L_p denotes the L_p spaces ($1 \leq p \leq \infty$) equipped with the norm $\| \cdot \|_{L_p}$, and H^k denotes the Sobolev spaces equipped with the norm $\| \cdot \|_{H_k}$. Details about Sobolev spaces can be found in ADAMS [1]. Geometric vectors are written in **bold-face**, and $| \cdot |$ denotes the Euclidean norm of such a vector. Similarly $\mathbf{L}_p$ and $\mathbf{H}^k$ denote the spaces of vector valued functions which components belong to L_p and H^k respectively.

2.1   The State Equation

Let $\Omega \subset \mathbb{R}^d$ ($d = 2,3$) be a fixed domain, the so called ground structure. Furthermore, we assume that Ω is an open, bounded connected domain with a Lipschitz boundary Γ. Moreover let $\Gamma_u \subset \Gamma$, $|\Gamma_u| > 0$ be the part of the boundary where the displacements are
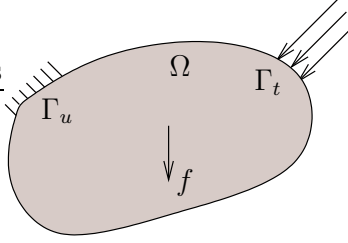
Figure 1: The reference domain and applied forces in a minimal compliance problem.

fixed, and $\Gamma_t = \Gamma \setminus \Gamma_u$ the part where boundary tractions are predescribed. Later on the optimal design is generated referring to this ground structure.

For describing material in Ω let $\rho \in L_\infty(\Omega)$ be a function representing the material density which fulfills $0 < \underline{\rho} \leq \rho \leq 1$ almost everywhere (a.e.) in Ω, where $\underline{\rho}$ is some positive lower bound. Then, let $\overline{E}^0_{ijkl}$ describe an elasticity tensor of fourth order, satisfying the usual symmetry, ellipticity and boundedness assumptions, representing a certain isotropic material. Further, let η be a monotonously increasing material interpolation function, mapping $[\underline{\rho}, 1]$ to $(0, 1]$, and describing how the actual density influences the elasticity tensor (e.g., to enforce 'black and white' designs) at a given point $\mathbf{x}$. More information about material interpolation is given in Section 3.1. Then the actually used elasticity tensor varies over the ground structure and is defined as

$$E_{ijkl}(\rho(\mathbf{x})) = \eta(\rho(\mathbf{x}))E^0_{ijkl}, \qquad \text{for } \mathbf{x} \in \Omega. \tag{1}$$

Here it is required that $\eta(1) = 1$ and that $0 < \eta(\underline{\rho}) \ll 1$, which describes a very compliant material pretending to be void.

Now for a fixed ρ and for a fixed η, the displacement field $\mathbf{u} \in \mathbf{V}_0$ fulfills the following equilibrium or state equation in its variational formulation:

$$a(\rho; \mathbf{u}, \mathbf{v}) = \ell(\mathbf{v}) \qquad \text{for all } \mathbf{v} \in \mathbf{V}_0, \tag{2}$$

where $\mathbf{V}_0 = \{\mathbf{v} \in \mathbf{H}^1(\Omega) \mid \mathbf{v} = \mathbf{0} \text{ on } \Gamma_u\}$ is the space of kinematically admissible displacements. The energy bilinear form on $\mathbf{V}_0 \times \mathbf{V}_0$ is defined as

$$a(\rho; \mathbf{u}, \mathbf{v}) = \int_\Omega E_{ijkl}(\rho(\mathbf{x}))\varepsilon_{ij}(\mathbf{u})\varepsilon_{kl}(\mathbf{v}) \, d\mathbf{x}, \tag{3}$$

with linearized strains $\varepsilon_{ij}(\mathbf{u}) = \frac{1}{2}\left(\frac{\partial \mathbf{u}_i}{\partial \mathbf{x}_j} + \frac{\partial \mathbf{u}_j}{\partial \mathbf{x}_i}\right)$ and the load linear form

$$\ell(\mathbf{v}) = \int_\Omega \mathbf{f} \cdot \mathbf{v} \, d\mathbf{x} + \int_{\Gamma_t} \mathbf{t} \cdot \mathbf{v} \, ds \tag{4}$$

defines a linear, bounded functional on $\mathbf{V}_0$, where $\mathbf{f} \in \mathbf{L}_2(\Omega)$ defines the body forces and $\mathbf{t} \in \mathbf{L}_2(\Gamma_t)$ describes the boundary tractions.

3

Again let η be fixed, but $\rho(\mathbf{x}) \in [\underline{\rho}, 1]$ arbitrary, then $a(\rho; \mathbf{u}, \mathbf{v})$ satisfies the following conditions (see, e.g., CIARLET [9]):

$$\exists \mu_1 > 0 : \quad \mu_1 \eta(\underline{\rho}) \|\mathbf{v}\|^2_{\mathbf{H}^1(\Omega)} \leq a(\rho; \mathbf{v}, \mathbf{v}), \quad \text{for all } \mathbf{v} \in \mathbf{V}_0, \tag{5}$$

which is due to Korn's inequality, and

$$\exists \mu_2 > 0 : \quad |a(\rho; \mathbf{u}, \mathbf{v})| \leq \mu_2 \|\mathbf{u}\|_{\mathbf{H}^1(\Omega)} \|\mathbf{v}\|_{\mathbf{H}^1(\Omega)}, \quad \text{for all } \mathbf{u}, \mathbf{v} \in \mathbf{V}_0.$$

For the $\mathbf{V}_0$-ellipticity (5) it is crucial that $\eta(\underline{\rho})$ is strictly positive. Assuming that the linear load form $\ell(\mathbf{v})$ fulfills the following boundedness criterion

$$\exists \mu_3 > 0 : \quad \|\ell\|_{\mathbf{V}_0^*} = \sup_{0 \neq \mathbf{v} \in \mathbf{V}_0} \frac{\ell(\mathbf{v})}{\|\mathbf{v}\|_{\mathbf{H}^1(\Omega)}} \leq \mu_3,$$

the total potential energy of the structure, given by a fixed ρ and the load form ℓ, can be stated as

$$J(\rho; \mathbf{v}) = \frac{1}{2} a(\rho; \mathbf{v}, \mathbf{v}) - \ell(\mathbf{v}),$$

with $J(\rho; \mathbf{v})$ strictly convex. The equilibrium displacement field $\mathbf{u}$ is now the unique minimizer of $J(\rho; \mathbf{v})$ with respect to $\mathbf{v} \in \mathbf{V}_0$, i.e. the principle of minimum potential energy or the principle of virtual work, when equivalently characterized as the solution of (2).

2.2 The Optimization Problem

The considered design problem consists now of minimizing the compliance (maximizing the stiffness) of a structure, with respect to the state equations (2) and some design constraints. For the sake of simplicity the body forces in (4) are omitted. Furthermore it is assumed that a proper material interpolation function η has been chosen. Mathematically the MCP can be formulated as the following optimization problem:

$$\min_{\rho \in L_\infty(\Omega), \mathbf{u} \in \mathbf{V}_0} \quad \ell(\mathbf{u}) \tag{6}$$

$$\text{subject to:} \quad a(\rho; \mathbf{u}, \mathbf{v}) = \ell(\mathbf{v}) \quad \text{for all } \mathbf{v} \in \mathbf{V}_0, \tag{7}$$

$$\int_\Omega \rho(\mathbf{x}) \, d\mathbf{x} \leq v_0, \tag{8}$$

$$\underline{\rho} \leq \rho(\mathbf{x}) \leq 1 \quad \text{a.e. in } \Omega, \tag{9}$$

Clearly the constraint (7) represents the state equations, the constraint (8) controls the volume of the used material, where v_0 is a positive bound on the used volume, and (9) ensures that the density stays within reasonable bounds.

In the above formulation the problem would lead to a simultaneous (all-at-once) approach, reducing the error of the constraining state equations is done at the same time as minimizing the objective. But usually, and also in this work, the state variable $\mathbf{u}$ is

eliminated through (7), resulting in a nested (black-box) approach. For a given admissible ρ the solution of (7) is exists and is unique and is denoted by $\mathbf{u}(\rho)$. So we arrive at the nested formulation of the minimal compliance problem:

$$\min_{\rho \in L_\infty(\Omega)} \qquad \ell(\mathbf{u}(\rho)) \tag{10}$$

$$\int_\Omega \rho(\mathbf{x}) \, d\mathbf{x} \le v_0, \tag{11}$$

$$\underline{\rho} \le \rho(\mathbf{x}) \le 1 \qquad \text{a.e. in } \Omega. \tag{12}$$

Now the state constraints (7) are hidden in the objective (10), which means that for every function evaluation or derivative calculation the state equations have to be solved in order to evaluate the nonlinear map $\rho \mapsto \mathbf{u}(\rho)$.

Both approaches, the simultaneous and the nested one, have advantages and disadvantages, but it is not within the scope of this report to discuss this, although it is a very interesting subject. Some results with respect to a simultaneous approach can be found, e.g., in HOPPE, PETROVA, AND SCHULZ [12] and MAAR AND SCHULZ [13].

2.3 Discretization using Finite Elements

When solving problems like (6) - (9) or (10) - (12) numerically they are usually discretized using finite elements on a triangulation $\mathcal{T}_h = \{\tau_i\}, i = 1, \ldots, n$ (see, e.g., CIARLET [9] or BRAESS [8] for an introduction the method of finite elements). Following a standard finite element procedure the ground structure Ω is partitioned into $n = O(h^{-d})$ $(n = N_{el} = N_\rho)$ triangles τ_i, where h is the used discretization parameter. For a more detailed description of the triangulation we refer to CIARLET [9]. It is worth noticing that there are two different variables, the displacements $\mathbf{u}$ and the density ρ. For both the same finite element mesh is used, but not the same finite elements.

The density ρ is approximated by a piecewise constant finite element function $\tilde{\rho}$, i.e. $\tilde{\rho}$ is constant over every triangle τ_i. The displacement field $\mathbf{u}$ is approximated as continuous element-wise quadratic functions and the finite element function $\tilde{\mathbf{u}}$ is now the the unique solution of the finite element equations:

$$a(\tilde{\rho}; \tilde{\mathbf{u}}, \tilde{\mathbf{v}}) = \ell(\tilde{\mathbf{v}}) \qquad \text{for all } \tilde{\mathbf{v}} \in \mathbf{V}_0^h, \tag{13}$$

where $\mathbf{V}_0^h = \mathcal{P}_2(\mathcal{T}_h)$ denotes the finite dimensional subspace of $\mathbf{V}_0$ and $\tilde{\rho} \in \mathbf{Q}^h = \mathcal{P}_0(\mathcal{T}_h)$. Here $\mathcal{P}_k(\mathcal{T}_h)$ denotes the space of polynomials of maximal degree k over the triangle τ_i. Whenever mesh refinement is performed it is done in such a way that $\mathbf{V}_0^h \supset \mathbf{V}_0^H$ if $h \le H$. Let the vectors $\mathbf{u}^h \in \mathbb{R}^{N_u}$ and $\boldsymbol{\rho}^h \in \mathbb{R}^n$ contain the coefficients of the finite element functions $\tilde{\mathbf{u}} \in V_0^h$ and $\tilde{\rho} \in Q^h$, respectively. Then, the discrete analogon of the state equations (2) turns from (13) to the following linear system of equations:

$$\mathbf{K}(\boldsymbol{\rho}^h)\mathbf{u}^h = \mathbf{f}^h \quad \in \mathbb{R}^{N_u}, \tag{14}$$

where, $\mathbf{f}^h$ denotes the load vector. The stiffness matrix $\mathbf{K}(\boldsymbol{\rho}^h)$ depends on the design vector $\boldsymbol{\rho}^h$ as follows:

$$\mathbf{K}(\boldsymbol{\rho}^h) = \sum_{i=1}^{n} \eta(\rho_i^h)\mathbf{K}_i, \tag{15}$$

where $\mathbf{K}_i$ are the element stiffness matrices extended to $N_u \times N_u$ matrices, which are weighted with the values of the material interpolation function evaluated at the elements densities.

Now, with $\mathbf{u}^h(\boldsymbol{\rho}^h)$ denoting the unique solution of (14), the discrete analogon of the continuous objective (10) is $\mathbf{f}^{h^T}\mathbf{u}^h(\boldsymbol{\rho}^h)$. Furthermore let the vector $\mathbf{v}^h$ represent the volumes of the finite elements such that $v_i^h = |\tau_i|$. Then the discrete version of the MCP can be posed as follows:

$$\min_{\boldsymbol{\rho}^h \in \mathbb{R}^n} \quad \mathbf{f}^{h^T}(\mathbf{u}^h(\boldsymbol{\rho}^h)) \tag{16}$$

$$\mathbf{v}^{h^T}\boldsymbol{\rho}^h \leq v_0, \tag{17}$$

$$\underline{\rho} \leq \rho_i^h \leq 1, \quad i = 1, \dots, n. \tag{18}$$

3 Material Interpolation Schemes and Regularization

3.1 Material Interpolation Schemes

Actually the basic question in the MCP is how to distribute a certain amount of material such that the resulting structure is as stiff as possible. So, for each point of the ground structure one has to decide whether to occupy it with material or not. In this terminology the continuous constraint (12) should be replaced by the discrete version $\rho(\mathbf{x}) \in \{\underline{\rho}, 1\}$ a.e. in Ω. But in order to avoid e.g. branch and bound techniques to solve the discretized '0-1' problem, the discrete valued constraint is relaxed to the continuous one. However, the design variable is then allowed to attain values between 0 (in fact $\underline{\rho}$) and 1, which is undesirable, and those intermediate values should be penalized to obtain again a more or less 0-1 or 'black and white' design.

By far the most popular penalization method is the so called SIMP (Solid Isotropic Material with Penalization) model, which has turned out to be extremely efficient. Here a nonlinear interpolation model of the following form is used:

$$\eta(\rho(\mathbf{x})) = \rho(\mathbf{x})^p, \qquad \text{with} \quad p \geq 1. \tag{19}$$

Intermediate values would then give very little stiffness in comparison to the amount of used material. In other words, by choosing a higher value than 1 for the parameter p, it is inefficient for the algorithm to choose intermediate density values.

An alternative approach to the SIMP method is the following interpolation model:

$$\eta(\rho(\mathbf{x})) = \frac{\rho(\mathbf{x})}{1 + q(1 - \rho(\mathbf{x}))}, \qquad \text{with} \quad q \geq 0. \tag{20}$$

This model is called RAMP, which stands for Rational Approximation of Material Properties. One disadvantage of SIMP versus RAMP is that the mass depends linearly on the element density ρ_i^h and the element stiffness depends on the power of ρ_i^h, which results in a non finite ratio of mass to stiffness when ρ_i^h attends zero. More information is given in BENDSØE AND SIGMUND [4], and a detailed motivation and introduction to the RAMP interpolation scheme can be found in STOLPE AND SVANBERG [16].

A totally different approach to penalize intermediate density values is to choose the material interpolation function $\eta(\rho(\mathbf{x})) = \rho(\mathbf{x})$ and to add an additional constraint to the optimization problem to encourage 'black and white' optimal designs. Such a penalty constraint could e.g. look like the following:

$$P(\rho(\mathbf{x})) = \int_{\Omega} (1 - \rho(\mathbf{x}))(\rho(\mathbf{x}) - \underline{\rho}) \, d\mathbf{x} \leq \varepsilon_P. \tag{21}$$

Of course such a penalty function could also be added as a penalty term to the objective functional.

3.2   Regularization

A naive formulation of topology optimization tasks like minimizing compliance will lead to difficulties due to the ill-posedness in the sense that there are no optimal solutions. The physical explanation is that given a structure with a certain volume, one can improve the stiffness by introducing lots of small holes without changing the actual volume, which will lead to an indefinite perforation of the structure. Mathematically speaking the reason for this effect is the non-closure of the feasible design set.

An optimization problem is said to be well-posed when the two following conditions are valid: The objective functional has to be lower semi-continuous and the feasible set has to be compact, and both properties have to be fulfilled with respect to the same topology. For the minimal compliance problem (10) - (12), the feasible set is weakly* compact in $L_\infty(\Omega)$. However, the objective functional is not weakly* lower semi-continuous in $L_\infty(\Omega)$ when the material interpolation function is chosen according to the SIMP or RAMP technique, in contrast to the original choice $\eta(\rho) = \rho$. But when using $\eta(\rho) = \rho$ and penalizing intermediate values like in (21), the set of feasible designs not weakly* closed anymore, see BORRVALL AND PETERSSON [6], and the problem lacks solutions again.

The effect that a larger number of holes appears and that more and more fine-scaled parts yield a more detailed structure, when solving the same problem on finer and finer grids, is called *mesh-dependence*. An illustration of the mesh-dependence effect can be seen in Fig. 2. Ideally refining the mesh should result in the same optimal design, but with a better and smoother description of the boundary. Basically there are two different ways to circumvent the ill-posedness, namely *relaxation methods* and *restriction methods*.

Relaxation methods in principle enlarge the feasible set of designs. Well-posedness is achieved by introducing an infinitely fine microstructure in every element of the structure and using the homogenized properties of these microstructures as material properties of
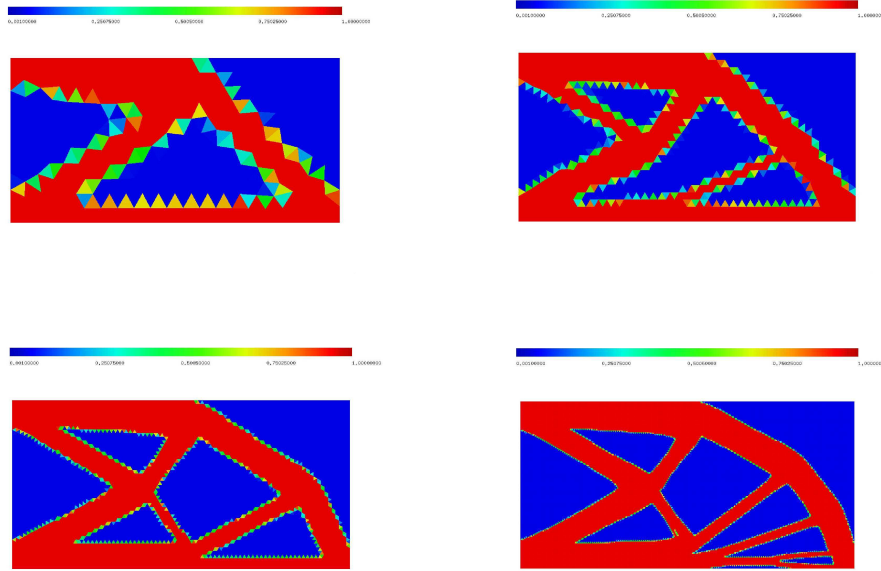
Figure 2: Mesh refinement without regularization. Solutions on a mesh with 449, 1839, 7319, and 29443 elements, respectively.

that element. A deeper insight of this *homogenization approach to topology optimization* is given by, e.g., BENDSØE AND SIGMUND [4].

In comparison with relaxation methods, restriction methods reduce the set of feasible designs, such that a sufficient closure is gained. Mainly this is achieved by adding one extra constraint to the problem, ruling out the possibility for fine scale structures to formate, or by using some filter techniques, filtering the sensitivities or directly the density. A survey of various restriction methods are given by BENDSØE AND SIGMUND [4], SIGMUND AND PETERSSON [15], BORRVALL [5] and BOURDIN [7].

Two different filter methods to restrict the design space are used in the calculations presented in this paper. The first one is called Regularized Intermediate Density Control (*RIDC*) and is discussed in detail in BORRVALL AND PETERSSON [6]. Here the material interpolation function is chosen as $\eta(\rho) = \rho$, such that the problem without any penalization of intermediate density values is well posed. But in order to calculate a black and white optimal design the intermediate density values are penalized by an additional constraint like (21). To get a sufficiently closed set of feasible designs, (21) is modified such that the design variable ρ is filtered firstly by a convolution operator S and then penalized via (21). Let $S : \mathbf{L}_2(\Omega) \to \mathbf{L}_2(\Omega)$ be an integral operator defined by

$$S(\rho(\mathbf{x})) = \int_{\Omega} \phi(\mathbf{x}, \mathbf{y})\rho(\mathbf{y}) \, d\mathbf{y}, \ \mathbf{x} \in \Omega. \quad \text{where} \tag{22}$$

where $\phi(\mathbf{x}, \mathbf{y}) = C(\mathbf{x}) \max(0, 1 - |\mathbf{x} - \mathbf{y}|/R)$ and $C(\mathbf{x})$ is chosen such that $\int_{\Omega} \phi(\mathbf{x}, \mathbf{y}) \, d\mathbf{y} = 1$.

8

Basically this means a linear convolution with a cone of base radius R. The penalizing constraint now looks as the following:

$$P(\rho) = \int_\Omega (1 - S(\rho(\mathbf{x})))(S(\rho(\mathbf{x})) - \underline{\rho}) \, d\mathbf{x} \le \varepsilon_P, \tag{23}$$

where a suitable value for ε_p must be found by experiments. Since this procedure is mostly very expensive, this is a serious disadvantage of this approach. But on the other hand for problems like the minimal compliance problem it is mathematically well founded (see BORRVALL AND PETERSSON [6]).

The second filter technique is used together with the RAMP interpolation scheme (20). Here not the density, but the discrete element sensivities of an objective J are modified as follows (e.g., see SIGMUND AND PETERSSON [15]):

$$\widehat{\frac{\partial J}{\partial \rho_k^h}} = \frac{1}{\rho_k^h \sum_{i=1}^n H_{i,k}} \sum_{i=1}^n H_{i,k} \rho_i^h \frac{\partial J}{\partial \rho_i^h}, \tag{24}$$

where the convolution operator $H_{i,k}$ with filter radius R is defined as

$$H_{i,k} = \max\left\{0, R - \operatorname{dist}(\tau_i, \tau_k)\right\}, \quad \text{for } i, k = 1, \dots, n.$$

The operator $\operatorname{dist}(\tau_i, \tau_k)$ represents the distance of the geometrical centroids of element τ_k and element τ_i. Roughly speaking this filter replaces the original derivatives by a weighted average of the derivatives in the surrounding area. The advantage of this filter approach is that it is very easy to implement and it turned out to work very well in various different topology optimization problems in 2D and in 3D. Moreover it is very robust with respect to coarse grids. But it must be pointed out that this filter is purely heuristic and it is not quite understood which problem is actually solved. In the following we will call this filter the *mesh-independence filter* and refer to it as *MIF*.

Both filter techniques are able to control the minimal length scale of the components in the optimal design. The larger the filter radius R is, the larger is the minimal length scale or the thicker are the occurring components, which is important, e.g., to ensure that the optimal structure is not too complicated to be manufactured. This influence of the filter radius can be seen in Fig. 3.

Another numerical anomaly is the so called *checkerboard effect*, which can be seen in Fig. 4. The appearance of checkerboard patterns is due to bad numerical modeling. For some combinations of finite element discretizations for the design ρ and the displacements $\mathbf{u}$ these patterns give an artificial high stiffness when analyzed in their discretized formulation. In the above mentioned citations a detailed explanation and various techniques to prevent these effects are described. Both filter methods mentioned above have the nice property to remove checkerboard effects or at least reduce them sufficiently.

4   A Multilevel Algorithm

Our basic motivation for a multilevel algorithm is to solve our problem efficiently and to save computational costs. This is achieved by solving the problem firstly on a coarse grid
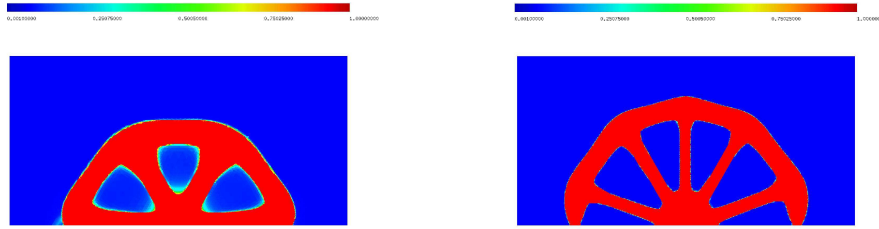
Figure 3: Different sizes of the filter radius: left $R = 0.15$ and right $R = 0.05$.
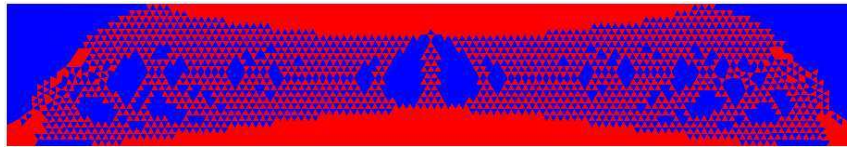

Figure 4: The checkerboard effect in the MBB beam example.

to get a first coarse design for rather cheap computational costs. Then we will use this first coarse design as an initial design on a finer grid and repeat the optimization on this finer grid, and so on. As the first coarse design is mostly close to the succeeding finer designs, this procedure will help us to avoid unnecessary long and expansive computations on very fine meshes.

4.1 Adaptive Mesh-Refinement

Since we want to solve our problem on a sequence of meshes $\{\mathcal{T}_l\}$ with a increasing number of elements, we have to address the question how to generate this sequence. Of course a basic idea would be to perform a uniform mesh-refinement, i.e. refine every element of the mesh. But proceeding this way would also introduce a lot of very fine elements in areas where a locally fine mesh is not needed. Elements inside a region full of material or void, far away from the structure's boundary, are very unlikely to be affected by the optimization on the next level. Far more interesting is the interface between void and material, i.e. the boundary of the design. It is much more efficient to identify this interface and only to refine the elements along this interface. In this way we ensure that new elements are inserted only where we need more detailed information. If material is moved, it will only happen around the boundary of the design, since no new holes will appear due to the regularization. Also finer elements along the interface give rise to the possibility that the boundary of the design can be described in a smoother way.

For identifying the interface the filter operator S defined in (22) turns out to be a useful tool. Let us consider a point $\overline{\mathbf{x}}$ in the design domain. If the function ρ is locally constant
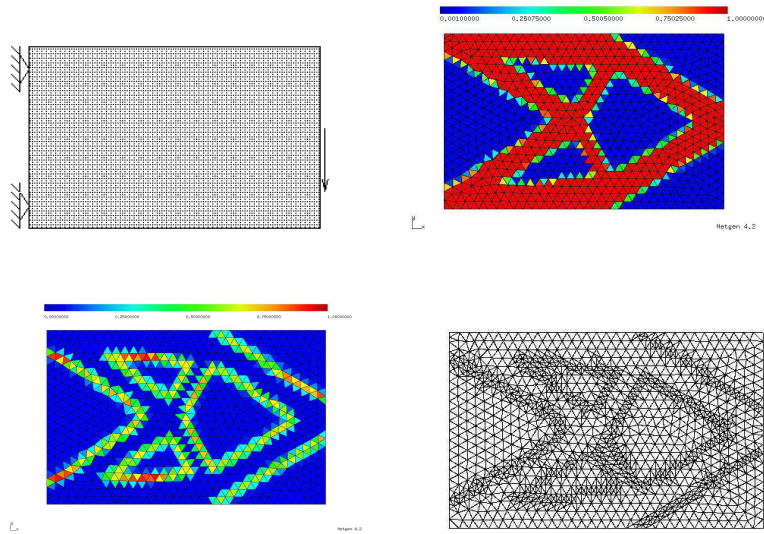
Figure 5: Sketch, coarse solution, identified boundary and refined mesh of the cantilever problem in 2D.

inside the filter region of $\overline{\mathbf{x}}$ (the support of the integral kernel $\phi(\overline{\mathbf{x}}, \mathbf{y})$ in (22)), then we have that $S(\rho)(\overline{\mathbf{x}}) = \rho(\overline{\mathbf{x}})$. If ρ is not constant inside the filter region, $|S(\rho)(\overline{\mathbf{x}}) - \rho(\overline{\mathbf{x}})|$ will have values different from 0. In fact $|S(\rho)(\overline{\mathbf{x}}) - \rho(\overline{\mathbf{x}})| \in [0, 1 - \underline{\rho}]$, since $S(\rho)(\mathbf{x}) \in [\underline{\rho}, 1]$ for $\mathbf{x} \in \Omega$ (see BORRVALL AND PETERSSON [6]). So we mark the element τ_i to be refined, if

$$|(\mathbf{\Phi}\boldsymbol{\rho}^h)_i - \rho_i^h| \geq \delta_1 > 0 \tag{25}$$

for some δ_1 with $1 \gg \delta_1 > 0$. Here $\mathbf{\Phi} \in I\!\!R^{n \times n}$ is the convolution matrix corresponding to the integral kernel ϕ. In Fig. 5 one can see the application of this refinement idea to the cantilever problem in 2D. In the upper line the sketch and the solution of the problem is shown. Then, in the lower line, in the left picture the identified interface using the refinement indicator (25) (scaled to [0,1]) and in the right picture the final refined mesh is plotted. Moreover, in Fig. 6 the refinement indicator for the cantilever problem in 3D is shown.

Varying the size of the filter radius R_{ref} for the refinement indicator we can control the sensivity of the indicator with respect to the interface. The larger we choose R_{ref} the more elements around the interface are chosen to be refined. But of course R_{ref} should be at least greater than the distance of all elements centroids to their at most $d + 1$ adjacent neighboring elements centroids:

$$R_{ref} \geq \delta_2 \cdot \max_{i=1,\ldots,n} \{ \text{dist}(\tau_i, \tau_k) \mid \tau_k \in NH(\tau_i) \}, \quad \text{with } \delta_2 > 1,$$

where $NH(\tau_i)$ should represent the set of the adjacent neighboring elements of element τ_i. In Fig. 7 two different refined meshes are shown, resulting from two different refinement filter radii R_{ref}.
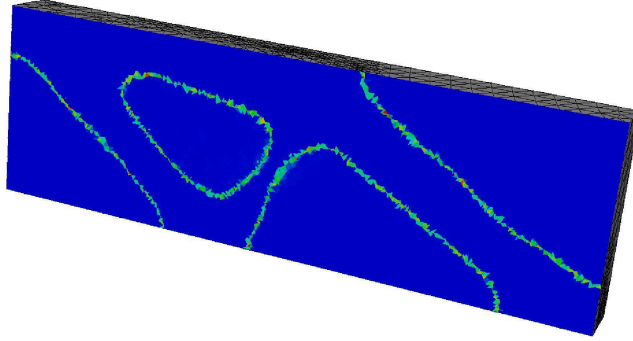
11

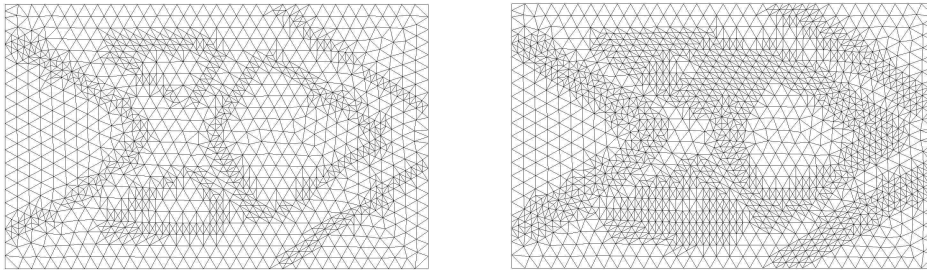Figure 6: The refinement indicator for the 3D cantilever problem.

Figure 7: Influence of the refinement filter radius R_{ref} on the refined mesh. Original mesh: 1463 elements. Left: Refined mesh with 2625 elements. Right: Refined mesh with 3741 elements.

4.2 A Multilevel Idea

In our multilevel approach we basically tried to combine the two filter methods mentioned in the last section, such that their disadvantages are eliminated and their advantages remain.

At the beginning the problem is solved on the coarsest grid $\mathcal{T}_0$. Here, at the first level, we use the mesh-independency filter MIF for regularization together with the RAMP interpolation scheme combined with a *continuation method*. The latter means that the RAMP-parameter q is slowly raised through the optimization progress. In the first few iterations $q = q_0$ is chosen, then for the next ones some higher value, until a wanted value q_{max} for q is reached where the design is finally fully optimized. The advantage of such a continuation method is that one avoids to get early stuck in an unwanted local minima, which may happen if the calculation is done only with one value of q, which is chosen too large. There are two major reasons why we use MIF combined with RAMP on the coarsest grid. On the one hand we can use coarser grids as with the RIDC method and on the other hand we can use the optimal design $\boldsymbol{\rho}^H$ of the coarsest grid to get a realistic value for ε_P in (23), setting $\varepsilon_P = P(\boldsymbol{\rho}^H)$. This saves us costly experiments to find a proper value for ε_P.

1: **Coarse grid solution** ρ^H with MIF and RAMP, $l = 0$.

2: **Determine $\boldsymbol{\varepsilon_P^0}$** by $\varepsilon_P^0 = P(\rho^H)$.

3: **Mesh-refinement** along the interface of 'void' and 'material'. Possible reduction of ε_P: $\varepsilon_P^{l+1} = \delta_3 \varepsilon_P^l$, $0 < \delta_3 \leq 1$.

4: **Fine grid solution** using RIDC.

5: **Satisfying solution?**
No: $l = l + 1$, $\rightarrow$ Step 3. Yes: STOP.

RAMP, MIF

Get ε_p
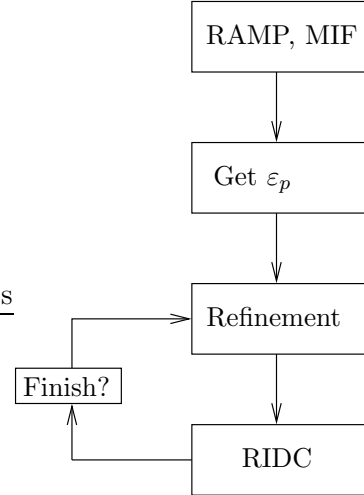
Refinement

Finish?

RIDC

Figure 8: Data flow of our multilevel algorithm.

Although we adapted the MIF formula (24) in an obvious way to work also on adaptively refined grids, we didn't achieve as good results as on uniformly refined grids.

So we continue on the refined grids with the RIDC method, which works fine on un-structured grids and is mathematically well-founded. Moreover, since the effective density and the original density ρ are the same ($\eta(\rho) = \rho$), there are no doubts which density is the one to plot. The basic data flow of this multilevel approach can be seen in Fig. 8.

In the optimal coarse grid design the interface $I = \{\mathbf{x} \in \Omega \mid \underline{\rho} < \rho(\mathbf{x}) < 1\}$ between void and material might have a quite significant width (a fuzzy interface). In order to minimize these zones of intermediate material we reduce ε_P from level to level like $\varepsilon_P^{l+1} = \delta_3 \varepsilon_P^l$ with $0 < \delta_3 \leq 1$. So the initial diffuse interface turns, as l increases, into a sharp interface. Unfortunately, if δ_3 is chosen too small, it may happen that the optimization algorithm is unable to find a feasible point at the next level $l+1$. The following choice of δ_3 turned out to work quite well, in fact it was successful with all our test examples:

$$\delta_3 = 1 - \frac{1}{2}\frac{\int_\Omega \chi_I(\mathbf{x})\rho(\mathbf{x})d\mathbf{x}}{\int_\Omega \rho(\mathbf{x})d\mathbf{x}},$$

where χ_I denotes the characteristic function of the interface I.

5 Numerical Experiments

We tested the approach described above with several known benchmark examples and got very good results from all of them. For solving the discrete optimization problem (16) - (18) we used the method of moving asymptotes (MMA), which is quite popular in the field of structural optimization. In MMA the original problem is solved iteratively by

sequential approximating subproblems, which are convex and separable. For the sake of space we will omit a detailed description of this method and refer the interested reader to SVANBERG [17, 18].
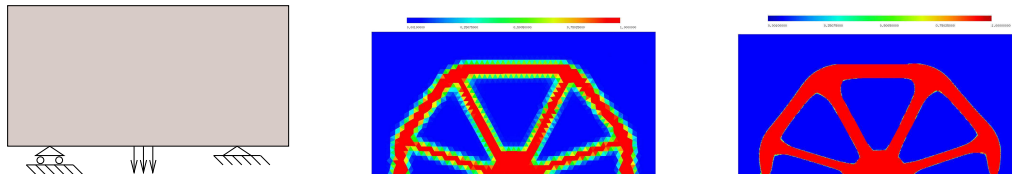

Figure 9: Sketch, coarse grid and fine grid solution of the 'wheel' example.

l	N_{el}	$N_{\mathbf{u}}$	t_{state}	t_∇	t_{opt}	t_{fil}	t_{it}	$Iter.$
level 0:	3334	13666	1.4	0.5	0.02	0.1	2.0	101
level 1:	7574	34908	3.7	1.2	0.05	0.3	5.6	76
level 2:	20661	100448	12.1	3.2	0.2	2.4	20.5	70
level 3:	46009	227248	27.6	7.1	0.5	15.2	66.3	49
level 4:	97648	485506	67.6	15.2	1.1	100.0	284.8	36
level 5:	213634	1065532	156.1	33.1	2.7	655.2	1519.4	16
level 6:	431476	2154826	329.4	67.2	6.7	4282.9	8991.2	11

Table 1: Computational data from the 2D wheel example.

In Table 1 we list the computational data gained from the 'wheel'-example. The columns N_{el} and $N_{\mathbf{u}}$ contain the number of finite elements and the degrees of freedom w.r.t. the displacements. The other columns t_{state}, t_∇, t_{opt}, t_{fil} and t_{it} show the time used for one evaluation of the state equation, of the derivatives, for the solution of the subproblem, for applying the filter and the overall time per iteration. In the last column the number of needed iterations is listed. We stopped the algorithm at each level when the maximum norm of the difference between two successive designs is less than 0.1 and the relative difference of two successive objective values was less then 10^{-5}. It turned out that this is a sufficiently tight convergence criteria for good design results. For solving the direct problem in 2D we used a fast sparse Cholesky factorization. To get an impression about the gained speed-up we also solved the problem on a uniform mesh $\mathcal{T}$ with 100889 elements. That is roughly the same number of elements as in the mesh $\mathcal{T}_4$ of level 4, and the optimization only on $\mathcal{T}$ took 176 iterations, which is an approximate time slow-down by the factor of 4 in comparison to the multilevel approach. But still the smallest elements of $\mathcal{T}_4$ (around the interface) are smaller as the ones in $\mathcal{T}$ by a factor of approximately 10.

We also applied this multilevel algorithm to other known 2D examples, where the solutions are shown in Fig. 10. In all 2D examples the available volume was restricted to $0.5|\Omega|$ and the filter radius was chosen as $R = 0.1$. The messurements of the ground
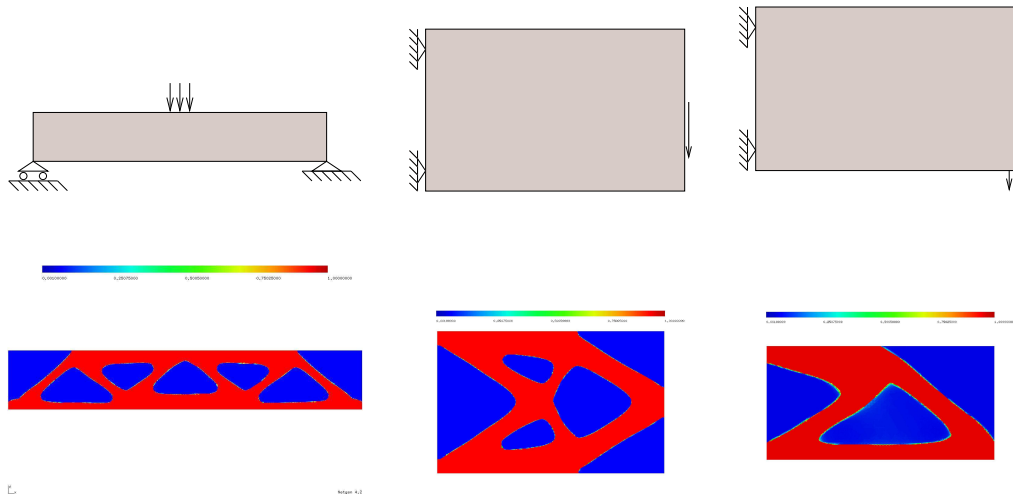
Figure 10: Sketch and fine grid solution of other 2D examples.

structures of the examples were 4×2, 6×1, 3.2×2 and 2×1 respectively. The time tables are basically the same, hence we omit them. Taking a close look at Table 1 we see that the used time for applying the filter is growing significantly, which is still a serious bottleneck for this approach. The same effect appears of course when calculating 3D examples, like the cantilever beam example. Fig. 11 shows sketch, coarse grid solution with 8100 elements and fine grid solution with 1101904 elements. Due to symmetry, the actual computation was performed only in a quarter of the domain. The available volume was $|\Omega|/3$, the filter radius was set to 0.5 and messurements of the the ground structure were $16 \times 10 \times 3$.
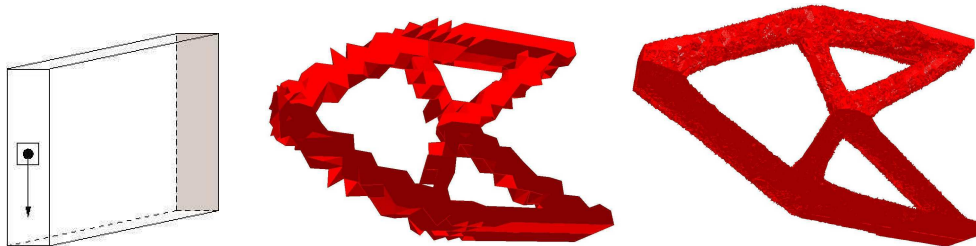

Figure 11: The cantilever beam in 3D: Sketch, coarse grid solution and fine grid solution.

Again, in Table 2, we list the computational data of the 3D example. In comparison to the direct solver for the 2D examples, we used here a multigrid preconditioned conjugate gradient method to solve the direct problem. As in the 2D examples it is possible to observe that the computational time for applying the filter operator grows quadratically. A comparison of the computational effort of applying the filter w.r.t. the solution of the state equation is plotted in Fig. 13. The used multigrid preconditioner so far does not take

15

l	N_{el}	$N_{\mathbf{u}}$	t_{state}	t_∇	t_{opt}	t_{fil}	t_{it}	$Iter.$
level 0:	2025	7224	2.6	1.1	0.01	0.0	3.8	88
level 1:	4615	15682	12.5	2.6	0.02	0.1	15.5	71
level 2:	11193	37048	32.1	6.2	0.06	0.8	40.9	49
level 3:	21604	70708	67.5	11.9	0.11	4.2	89.2	42
level 4:	39599	127806	130.4	21.8	0.23	16.9	187.5	27
level 5:	86279	274322	311.3	47.8	0.57	111.4	605.1	23
level 6:	141714	447432	595.7	78.4	1.01	381.1	1442.3	16
level 7:	275476	861462	1281.2	159.3	2.14	1680.8	4814.6	14

Table 2: Computational data from the 3D cantilever beam example.

into account the special structure of the state problem, the different scaling of the entries in the stiffness matrix w.r.t. void and material and the slightly changing interface per level. Per iteration a V-cycle with one pre- and post-smoothing step is done. Nevertheless, this results in an almost linear time complexity.
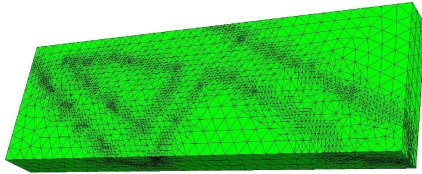

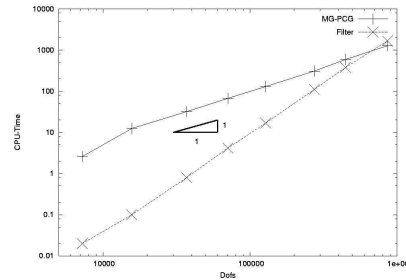Figure 12: Finally refined mesh of the 3D cantilever beam.

Figure 13: Applying the filter vs. solution of the state equation.

In Fig. 14 and 15 we see the result of another 3D example. As before, the computation was just done in a quarter of the domain. Since the computational data is similar to the one listed in Table 2, it is omitted again. Here the coarse grid solution is computed with 30236 (7559) elements and the fine grid solution with 608340 elements corresponding to 608340 (152085) design unknowns and 953964 (238491) displacement unknowns, respectively. All computations were performed on a computer with a 2.4 GHz CPU and 2 GB memory.

6   Conclusions and Outlook

In our multilevel approach we combined two filter techniques such that their disadvantages are eliminated and we gain from their good properties. Finally we ended up with an
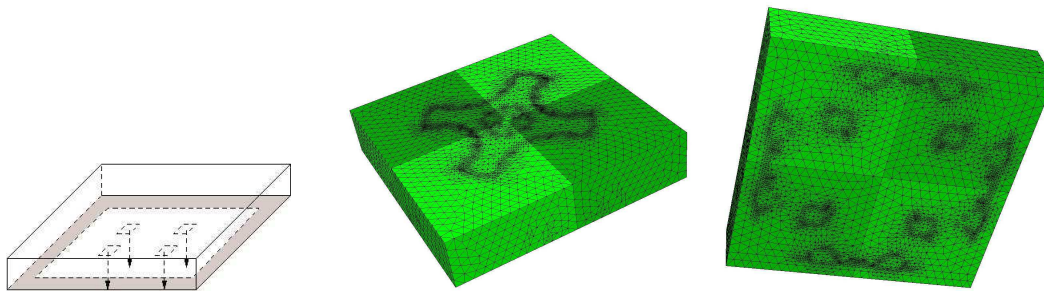
Figure 14: The 'roof' example: sketch and the finally refined mesh, once from above and below.

Figure 15: Coarse grid solution and fine grid solution.

efficient method to solve minimal compliance problems with a high resolution of elements around the interface between void and material in 2D and in 3D.

But still there is the serious bottleneck of the high complexity of applying the filter operator on adaptively refined triangular meshes. Here, a more efficient way has yet to be investigated for very fine resolutions. Also a point of high interest will be the investigation and construction of an optimal muligrid based solver for the state problem, taking into account the interface between material and void. Here we refer to a forcoming paper.

The implementation of this optimization algorithm is based on the software package NETGEN/NGSolve by J. Schöberl (see http://www.hpfem.jku.at), a very powerful meshing and finite element software tool.

References

[1] R.A. Adams. *Sobolov Spaces.* Academic Press, New York, 1976.

[2] G. Allaire. *Shape Optimization by the Homogenization Method.* Springer, New York Berlin Heidelberg, 2002.

[3] M. P. Bendsøe. *Optimization of Structural Topology, Shape and Material.* Springer, Berlin Heidelberg, 1995.

[4] M. P. Bendsøe and O. Sigmund. *Topology Optimization: Theory, Methods and Applications.* Springer, Berlin Heidelberg, 2003.

[5] T. Borvall. Topology optimization of elastic continua using restriction. *Archives of Computational Methods in Engineering*, 8:351–385, 2001.

[6] T. Borvall and J. Petersson. Topology optimization using regularized intermediate density control. *Computer Methods in Applied Mechanics and Engineering*, 190:4911–4928, 2001.

[7] B. Bourdin. Filters in topology optimization. *International Journal for Numerical Methods in Engineering*, 0:1–17, 2000.

[8] D. Braess. *Finite Elements: Theory, Fast Solvers and Applications in Solid Machanics.* Cambridge University Press, 1997.

[9] P. G. Ciarlet. *The Finite Element Method for Elliptic Problems.* North-Holland, Amsterdam, 1978.

[10] H.A. Eschenauer and N. Olhoff. Topology optimization of continuum structures: A review. *Applied Machanics Rev*, 54(4), 2001.

[11] J. Haslinger and P. Neittaanmäki. *Finite Element Approximation for Optimal Shape Design, Material and Topology Design.* John Wiley & Sons, Chichester, 1997.

[12] R.H.W. Hoppe, S.I. Petrova, and V. Schulz. A primal-dual newton-type interior-point method for topology optimization. *Journal of Optimization, Theory and Applications*, 114:545–571, 2002.

[13] B. Maar and V. Schulz. Interior point multigrid methods for topology optimization. *Structural and Multidisciplinary Optimization*, 19:214–224, 2000.

[14] G.I.N. Rozvany. Aims, scope, methods, history and unified terminology of computer-aided topology optimization in structural mechanics. *Structural and Multidisciplinary Optimization*, 21:90–108, 2001.

[15] O. Sigmund and J. Petersson. Numerical instabilities in topology optimization: A survey on procedures dealing with checkerboards, mesh-dependencies and local minima. *Structural and Multidisciplinary Optimization*, 16:68–75, 1998.

[16] M. Stolpe and K. Svanberg. An alternative interpolation scheme for minimum compliance topology optimization. *Structural and Multidisciplinary Optimization*, 22:116–124, 2001.

[17] K. Svanberg. The method of moving asymptotes - a new method for structural optimization. *International Journal for Numerical Methods in Engineering*, 24:359–373, 1987.

[18] K. Svanberg. A class of globally convergent optimization methods based on conservative convex separable approximations. *SIAM Journal of Optimization*, 12(2):555–573, 2002.